Engineering Fracture Mechanics 290 (2023) 109457

Contents lists available at ScienceDirect

Engineering Fracture Mechanics

journal homepage: www.elsevier.com/locate/engfracmech

Effect of the pre-crack non-uniformity on the initiation of brittle fracture in mini-CT specimen

Meng Li [a,b,*], Inge Uytdenhouwen [a,*], Thomas Pardoen [b], Rachid Chaouadi [a], Marlies Lambrecht [a]

[a] Belgian Nuclear Research Centre (SCK CEN), NMS Unit, Boeretang 200, 2400 Mol, Belgium

[b] Université catholique de Louvain, Institute of Mechanics, Materials and Civil Engineering (IMMC), Place Sainte Barbe, 1348 Louvain-la-Neuve, Belgium

ARTICLE INFO

Keywords:
Mini-CT
Pre-crack front non-uniformity
Brittle fracture
Local approach
Size restrictions

ABSTRACT

Non-uniform pre-crack fronts often develop during fatigue pre-cracking of mini-CT specimen, resulting in invalid measurement when following the tight requirements of the ASTM standards regarding fatigue pre-crack curvature. Invalid measurements lead to a waste of test resources which is a major issue for irradiated materials. Previous studies have demonstrated a weak effect of excessive pre-crack curvature on the experimentally measured fracture toughness in the transition regime. In this paper, experimental investigations as well as finite element simulations were performed to provide additional confirmation of this conclusion. In order to demonstrate that meaningful results can still be generated in the brittle regime from non-uniformly pre-cracked mini-CT specimens, a local approach of brittle fracture was adopted to quantify the effect of pre-crack front non-uniformity on the initiation of brittle fracture. The final goal is to contribute to consolidate relevant requirements on the pre-crack front curvature.

1. Introduction

The miniaturized compact tension geometry (mini-CT) has attracted worldwide attention for more than a decade as an appealing [1–3] miniaturized geometries in the determination of fracture toughness of the nuclear reactor pressure vessel (RPV) steels. Fig. 1 shows that eight mini-CT specimens can be easily machined out of two broken halves, and this cutting scheme makes the reorientation of the specimen possible. Most importantly, this geometry has been qualified to produce equivalent fracture toughness results [3–6].

As already outlined in a companion paper [7], although the mini-CT geometry has proved effective for the direct characterization of fracture toughness, a major potential limitation is the increased likelihood of non-uniform pre-crack front development during fatigue pre-cracking, which can be attributed to the reduction of specimen thickness. A crack front is considered as uniform when the a_0/W-ratio is relatively constant along the crack front. By contrast, a non-uniform crack front experiences significant variations of the a_0/W-values along the crack front. Experimentally, we cannot generate a perfectly straight crack with a_0/W equal to 0.5 at each location along the crack front. The ASTM standard provides a lower and upper bound delimiting the validity of the crack front with respect to crack straightness. According to ASTM E1921 [8], the specimen is considered invalid if any of the 9 individual physical measurements of the initial crack size differ by more than a validity limit set as $0.1(b_0B_N)^{1/2}$ (where b_0 is the initial ligament size, B_N is the net

* Corresponding authors at: Belgian Nuclear Research Centre (SCK CEN), NMS Unit, Boeretang 200, 2400 Mol, Belgium.
E-mail addresses: meng.li1991@outlook.com (M. Li), iuytdenh@sckcen.be (I. Uytdenhouwen).

https://doi.org/10.1016/j.engfracmech.2023.109457
Received 31 December 2022; Received in revised form 24 June 2023; Accepted 30 June 2023
Available online 1 July 2023
0013-7944/

specimen thickness), from the average crack length. The validity limit is typically more stringent for sub-sized test specimens, as it is directly linked to ligament size and specimen thickness, with a typically ± 0.4 mm tolerance range. As a result, a large number of mini-CT specimens are identified invalid due to excessive pre-crack front curvature, which is considered as an unnecessary waste of experimental data especially considering costly irradiated specimens. Previous studies by Lambrecht et al. [6] demonstrated a weak effect of invalid non-uniform pre-crack configuration on the experimentally measured fracture toughness in the brittle regime, and suggested that appropriate relaxation should be applied to the strict pre-crack curvature requirements in ASTM E1921-19b for miniaturized geometries to efficiently use the “invalid” test data that was excluded from T_0 evaluation.

In this study, the effect of pre-crack non-uniformity is addressed in the context of the brittle fracture regime. The first part of the paper investigates the effect of pre-crack non-uniformity in terms of macroscopic parameters, in which a comparison is conducted between mini-CT specimens with uniform straight pre-crack and tilted pre-crack. The tilted pre-crack front was specifically selected to allow sampling various a_0/W along the crack front and because it can easily be experimentally produced. Emphasis will be put on the local mechanical conditions in the near crack tip region that directly controls the initiation of brittle fracture, such as J-integral, maximum principal stress and fracture process zone size. The second part of the paper aims at studying the effect of pre-crack non-uniformity on the initiation of brittle fracture and subsequent fracture toughness evaluation using a local approach to brittle fracture incorporating plastic strain effects. The framework begins by validating the ability of the local approach to account for the effect of the pre-crack size, followed by the prediction of the scale fracture toughness, K_0, and the evaluation of the transition temperature, T_0, for uniform and non-uniform pre-crack configurations.

The main objective is to investigate the magnitude of the impact of pre-crack non-uniformity on crack initiation, thereby providing evidence for previous experimental studies from the perspective of finite element analysis. A local approach to brittle fracture is used to quantify the potential effects and to contribute to the consolidation of the existing requirements in ASTM E1921 regarding the level of acceptable pre-crack front curvature.

2. Experimental observations

The ASTM E1921-19b [8] specifies that the K_{Jc} value should be considered invalid if any of the physical measurements of the initial crack size according to the nine-point procedure exceeds by more than $0.1(b_0B_N)^{1/2}$ the average value. The previous version of the ASTM standard, E1921-18a [9] assumes a straight pre-crack front with a deviation of less than 5% from the average of the thickness dimension B, or 0.5 mm, whichever is larger. In terms of dimensions, the newer specification is about 75% relaxed compared to the previous most stringent limit, 5%B, but it is 25% stricter than the more lenient limit of 0.5 mm for a mini-CT specimen. At SCK CEN, the dimensional information and the test data of over 500 mini-CT specimens are included in a database that was used to investigate the effect of the specifications regarding the pre-crack curvature on the qualification of the test data [6]. Table 1 provides the number of valid and invalid specimens verified using the existing ($0.1(b_0B_N)^{1/2}$) and previous (5%B or 0.5 mm) pre-crack curvature criteria. By examining the validity of the pre-crack front curvature of 504 mini-CT specimens, it is found that 11.9% of the mini-CT specimens must be considered invalid based on the pre-described specification, which is a significant decrease compared to the invalid percentage of 53% based on the previous more stringent specification. However, it is higher than the 4% of invalid specimens under the previous, more lenient specification, which is typically used for mini-CT geometries. This indicates that quantitatively, the newer restriction on the pre-crack front curvature becomes even more stringent when applied to mini-CTs, and as a result, compared to the situation of large CT specimens, it eliminates a considerable number of mini-CT specimens that might have provided effective fracture toughness values.

Previous experimental results demonstrated that the pre-crack non-uniformity has a very weak effect on the fracture toughness of the mini-CT specimens [1,6]. In particular, real cracks (hydrogen flakes) with non-uniform front were compared to fatigue pre-crack with uniform front were found to negligibly affect fracture toughness measurements and the master curve reference temperature [1]. Similarly, tests performed on mini-CT specimens of 22NiMoCr37 steel where valid and invalid crack fronts were compared shown no significant difference on fracture toughness and master curve reference temperature [6]. Finally, preliminary finite element simulations, without using local approach of fracture, indicated also that the expected effect on non-uniform pre-crack front remains negligibly small [10] and confirmed recently by [11]. Since the previous work conducted using the SCK CEN database was carried out in accordance with the standards ASTM E1820-18 and ASTM E1921-18a where the validity limit of ± 5%B or 0.5 mm is applied, the 51 mini-CT specimens tested in the transition range were re-analyzed based on the pre-described updated restriction. Meanwhile, due to

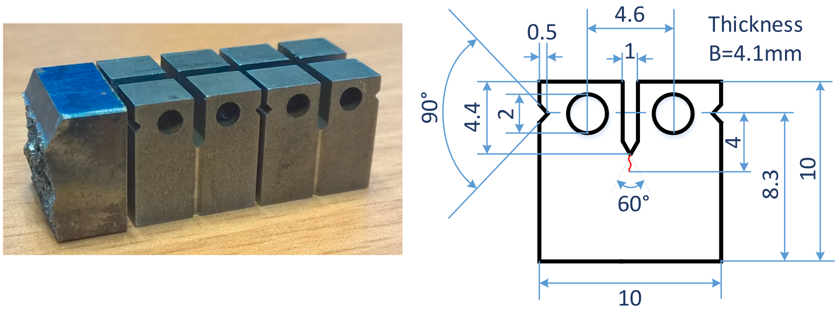

Fig. 1. Geometry and dimensions of mini-CT specimen.

Table 1
Summary of the validity of the mini-CT specimens regarding the pre-crack front curvature.

		All	Valid	Invalid	Invalid percentage (Invalid/All)
Validity limit	5%B	504	237	267	53.0%
	0.5 mm	504	484	20	4.0%
	$0.1(b_0B_N)^{1/2}$	504	444	60	11.9%

the very small proportion of invalid specimens when using the limit of 0.5 mm, it is difficult to detect the invalid specimens in the analyzed 51 20% side-grooved mini-CTs and therefore unable to demonstrate the impact of pre-crack front non-uniformity. Therefore, in order to fully capture the effect of pre-crack non-uniformity with an experimental basis, we will also analyze the condition when the limit of 0.5%B is employed. Table 2 shows the transition temperature, T_0, computed using valid and invalid data sets based on different validity limits. The results show that based on the previous validity limit, the computed T_0 values of three data sets: all data, valid data only and invalid data only show an overall good agreement. Then considering the pre-described validity limit, $0.1(b_0B_N)^{1/2}$, the T_0 computed from the invalid data set shows larger value, the difference in T_0 is outside the uncertainty band of the T_0 generated from all available data. However, one should indicate that the size of the invalid data set ($N = 6$, $r = 4$) is far below the required minimum number of mini-CT specimens required ($N = 12$) to define a reliable transition temperature. The T_0 obtained from this limited data set should not be considered reliable, as statistical effects could be the main reason for the bias. This issue requires further in depth finite element analysis based investigations. Fig. 2 shows the plots of the 1T-normalized K_{Jc} values of mini-CT geometry at different temperature, where, the valid and invalid data points are separated according to the validity limit of 5%B (Fig. 2-a) and $0.1(b_0B_N)^{1/2}$ (Fig. 2-b). As shown in Fig. 2(b), the test data at −150 °C are excluded in the case of the analysis of the invalid data points ($T_0 = -82$ °C) due to the test temperature allowance ($T_{test} = T_0 \pm 50$ °C) in ASTM E1921, the larger computed T_0 of the invalid data set is caused by the two low data points at −120 °C. Moreover, it should be noted that these two data points do not necessarily indicate that a non-uniform pre-crack configuration tends to produce lower fracture toughness. This is because the position of the invalid data points at −130 °C and −150 °C in Fig. 2(b) and the invalid data points distribution at each temperature in Fig. 2(a) show that it is difficult to distinguish the invalid data from the valid one. Therefore, the above experimental measurements, especially those obtained with 5%B, show that the fracture toughness data obtained from mini-CT specimens with pre-crack fronts that do not fulfill the crack front curvature requirements will not deviate significantly.

3. Finite element procedures

The following sections provide explanations based on finite element simulations for the above experimental observations by investigating the effect of pre-crack non-uniformity. The introduction of a local approach to brittle fracture makes it possible to quantify such effects, thus allowing the evaluation of the existing requirements on the pre-crack curvature. It should be noted that the selected non-uniform pre-crack in this study is voluntarily exaggerated in order to provide direct evidence of its effect. The non-uniform pre-crack in a real mini-CT specimen is much smoother with one or two points, generally close to the free surfaces of the specimen, below the lower validity limit. Thus, in practice, the effect of an invalid non-uniform pre-crack may not be so obvious, which depends on the actual shape of the pre-crack.

3.1. Elastoplastic properties

The material addressed in this study is a typical reactor pressure vessel (RPV) steel 22NiMoCr37, the chemical composition is given in Table 3. Mini round tensile bars with 15 mm gauge length and 3 mm diameter were tested to provide the hardening law. Because the present study mainly focuses on the ductile-to-brittle transition (DBT) region, the mechanical tensile tests were performed at a low temperature close to T_0, defined by $T_{test} = -110$ °C. The true stress–strain curve for the FEM simulations was then generated from the tensile test data, Bridgman's stress correction [12] has been applied to give an approximation of the equivalent true stress at fracture. The true stress–strain curve of 22NiMoCr37 at −110 °C is given in Fig. 3, the corresponding mechanical properties are given in Table 4.

Table 2
Summary of the T_0 determination based using different validity limits and data sets.

	Validity limit					
	5%B			$0.1(b_0B_N)^{1/2}$		
	All	Valid	Invalid	All	Valid	Invalid
N	51	12	39	51	45	6
r	39	8	31	39	33	4
T_{test} range, °C	−150 ~ -115	−150 ~ -115	−150 ~ -115	−150 ~ -115	−150 ~ -115	−150 ~ -115
T_0, °C	−106.7	−112.7	−104.6	−106.7	−108.6	−82.0
$1\sigma_{T0}$, °C	5.0	7.5	5.2	5.0	5.2	10.8

N = total number of the test data, r = number of the uncensored data.

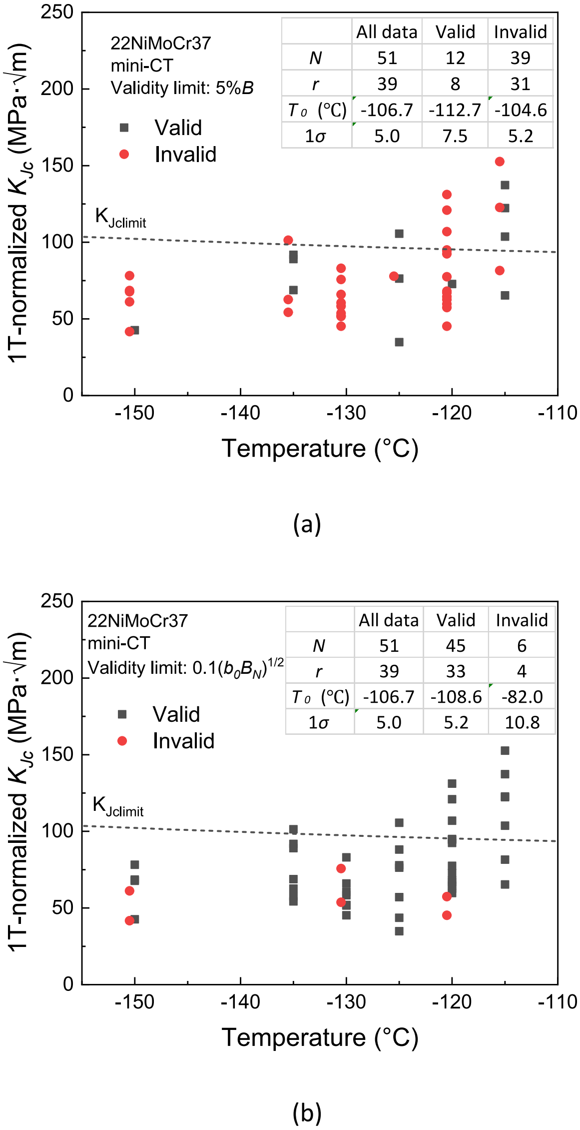

Fig. 2. Valid and invalid fracture toughness data points of mini-CT geometry based on (a) 5%B validity limit and (b) $0.1(b_0B_N)^{1/2}$ validity limit. ("1T-normalized K_{Jc}" is the 1 in. equivalent of measured K_{Jc}).

Table 3
Chemical composition (weight %).

Material	C	Si	Mn	S	P	Cr	Ni	Mo	Cu
22NiMoCr37	0.22	0.23	0.88	0.004	0.006	0.39	0.84	0.51	0.08

3.2. Finite element model

Non-linear finite element simulations were conducted for the 3-D model of the mini-CT specimen using the commercial package ANSYS. The geometry of mini-CT specimen model (see Fig. 4) is identical to the real experimental specimen that is used at SCK CEN as shown in Fig. 1, with $W = 8.3$ mm, $B = 4.1$ mm, $a_0/W = 0.5$ and 20% side grooves. Due to the symmetry conditions and the need to model non-uniform pre-crack configurations, one-half of the 3-D finite element model with a symmetric boundary imposed on the remaining ligament plane was used for the analysis. The mini-CT model was loaded by applying displacement increments to the pin model, which was modeled as a rigid body. Contact elements were applied between the specimen and the pin to simulate the interaction.

Additional attention was focused on the mean crack tip region. The meshing around the crack tip was highly refined, by using a

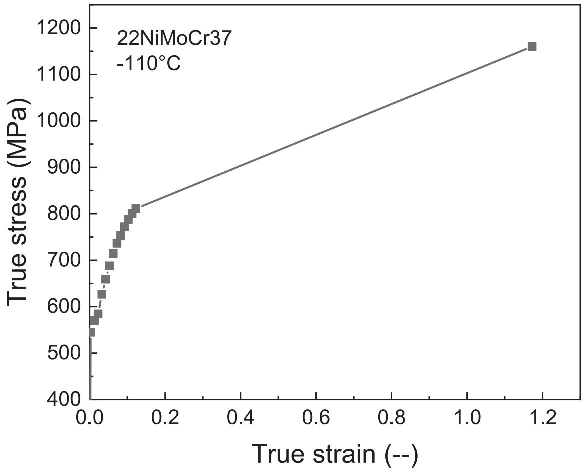

Fig. 3. Experimental true stress and true strain curve for the 22NiMoCr37 steel at −110 °C.

Table 4
Mechanical properties.

Material	*T* (°C)	*E* (GPa)	ν	σ_0 (MPa)	ε_{uts}	σ_{uts} (MPa)	$\sigma_{F,Bridgman}$(MPa)
22NiMoCr37	−110	213.6	0.3	577	0.139	719	1160

T = test temperature, E = Young's modulus, ν = Poisson ratio, σ_0 = yield strength, ε_{uts} = uniform elongation, σ_{uts} = ultimate tensile strength.

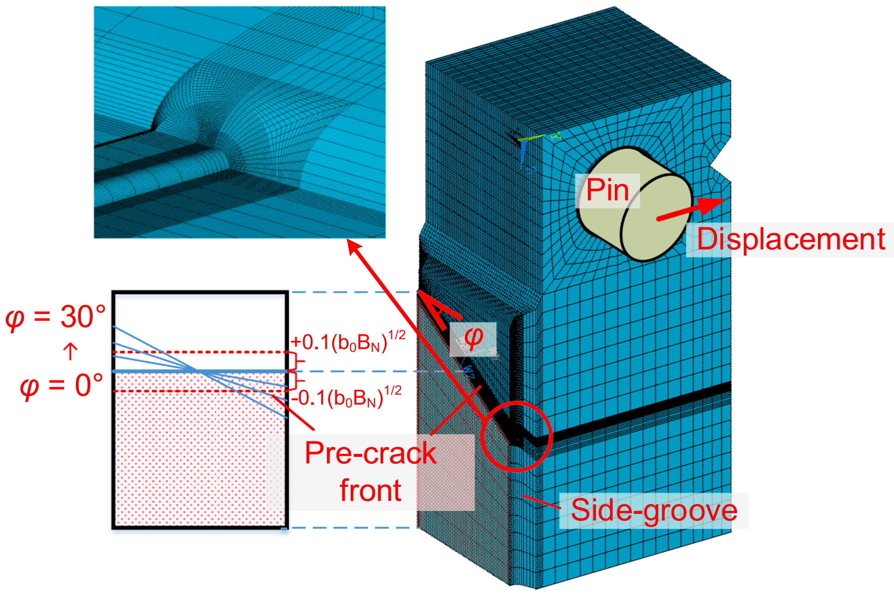

Fig. 4. Finite element model of mini-CT specimen.

"spider web" [13] mesh configuration with concentric rings of quadrilateral elements to ensure the evaluation of the local *J*-integral. The fatigue pre-crack was modeled as a straight initial notch with adjustable tilt angle. It was found in past studies, that the potential effects of the initial crack-tip notch radius on the stress and strain fields at the near tip region is negligible when the notch radius is small enough. A general suggestion is to keep the initial crack-tip notch radius at least 5 times lower than the CTOD at fracture initiation [14–17]. In addition, subsequent investigations on the local approach to brittle fracture also showed that almost identical

Weibull stress, σ_w, is provided by the configurations with $\rho_0 = 0.005$ mm and $\rho_0 = 0.01$ mm. Therefore, the effect of notch radius was considered to be limited, and if any, it can be compensated by sufficient mesh refinement. However, it should be noted that an extremely small notch radius is also undesirable because it may lead to unexpected extensive element distortion at the near tip region, such as a value of $\rho_0 = 0.0025$ mm [16,18]. Consequently, in the present study, the notch radius at the pre-crack tip, ρ_0, was fixed to be 0.005 mm (5 μm). J_2 flow theory based on a power law was assumed for the 22NiMoCr37 steel at −110 °C (values of the parameters are given in Table 4)

$$\frac{\sigma}{\sigma_{ys}} = \begin{cases} \frac{E\varepsilon}{\sigma_{ys}} & when\ \sigma < \sigma_{ys} \\ \left(1 + \frac{E\varepsilon^{pl}}{\sigma_{ys}}\right)^n & when\ \sigma > \sigma_{ys} \end{cases} . \tag{1}$$

4. Effect of pre-crack non-uniformity on macroscopic parameters

Finite element simulations were carried out to provide additional evidence for this limited effect of pre-crack non-uniformity. In

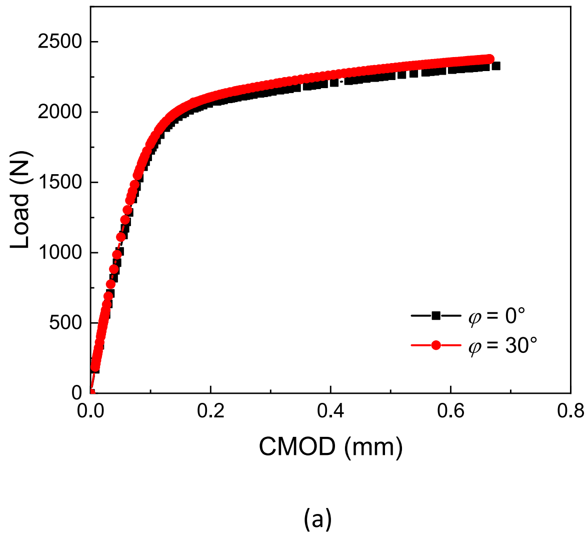

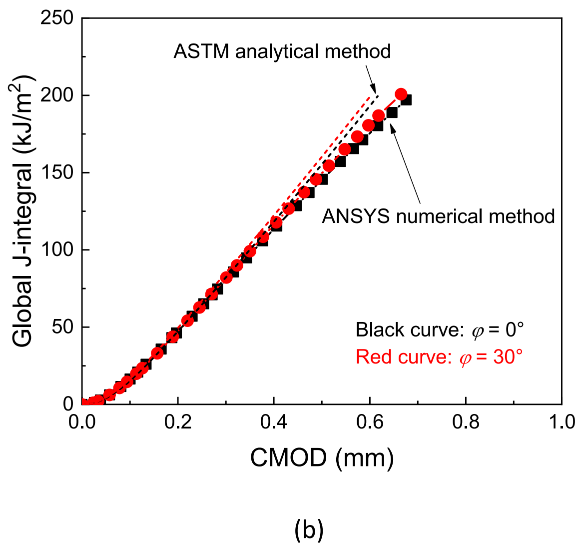

Fig. 5. Variation as a function of CMOD of (a) the applied load of mini-CT specimen with uniform and tilted pre-crack front (b) of the global *J*-integral of mini-CT specimen with uniform and tilted pre-crack front.

this section, attention is mainly focused on the effect of pre-crack non-uniformity on the macroscopic parameters that can be directly measured from fracture toughness tests, such as the applied load and J-integral, and that has direct impact on the initiation of brittle fracture, such as the maximum principal stress (σ_{yy}) and the fracture process zone size.

Fig. 5(a) displays the change in the applied load on the mini-CT specimen with increased crack mouth opening displacement (CMOD). Both the mini-CT specimen models with the uniform pre-crack front ($\varphi = 0°$) and the tilted pre-crack front ($\varphi = 30°$) are considered. As a pre-crack with an excessive inclination that violates the ASTM specification for the pre-crack front curvature, the 30° tilted pre-crack configuration can still provide similar maximum load which is less than 3% compared to that obtained from a uniform pre-crack configuration. The pre-crack non-uniformity is therefore demonstrated to have limited effect on the maximum loading. Fig. 5 (b) compares the global *J*-integral that is directly evaluated from the near tip region of the finite element model. The global *J*-integral computed here is the average value of the local *J*-integral estimated at each uniformly distributed position along the thickness. The finite element simulations provide a domain integral method by Shih [19,20], which offers a good accuracy and allows the evaluation of the local *J*-integral at each node over a number of integral contours around the crack on the plane normal to the crack front. The local *J*-integral at each node is extracted over more than 48 contours in order to precisely check the path independence. It can be seen from Fig. 5(b), the global *J*-integral generated from two extreme pre-crack configurations ($\varphi = 0°$ and 30°) show close agreements in the *J*-integral range that is often observed in the experiments at −110 °C. Two additional dotted curves showing the evolution of the global *J*-integral of two pre-crack configurations computed using the analytical method in the ASTM E1820 based on the load-CMOD data are also plotted. Both configurations provide close global *J*-integral results. These results demonstrate that the effect of pre-crack non-uniformity on the global driving force (maximum load and global *J*-integral) can be considered negligible even if excessive tilted pre-crack configuration is considered. The close agreement of the results computed using the ASTM analytical method and the ANSYS numerical method also indicates that both *J*-integral evaluation methods are equally acceptable.

In addition, attention here is directed towards the possible effect of the pre-crack non-uniformity on local mechanical conditions, involving the distribution of local *J*-integral over the pre-crack front. Three load levels within a reasonable range of the fracture toughness at −110 °C are considered: $J = 20$, 45 and 70 kJ/m^2, with corresponding K_{Jc} equal to 70, 100 and 130 MPa$\sqrt{\text{m}}$, respectively. Note that the *J*-integral is determined by ANSYS based on the domain integral method proposed by Shih [19,20], where the local *J*-integral at each node is extracted over more than 48 contours in order to precisely check the path independence. The K_{Jc} values are derived from the *J*-integral using the standard relationship that is introduced in section 9.1.5 of ASTM E1921 [8]. These K_{Jc} values indicate three different yielding conditions from small scale yielding to large scale yielding, as revealed in Fig. 6, which plots the evolution of the maximum stress triaxiality in front of the pre-crack with increased load level. It reveals that the small scale yielding condition ends at K_{Jc} equal to 88 MPa$\sqrt{\text{m}}$, then followed by large scale yielding condition. As plotted in Fig. 7, significant difference is observed from the local *J*-integral distribution over uniform and tilted pre-crack front. First of all, both of the pre-crack configurations experience a decrease of the local *J*-integral value when the plane stress condition is approached at the free surfaces. For the uniform pre-crack configuration, the local *J*-integral is almost uniformly distributed over a large portion of the pre-crack front, particularly under small scale yielding condition. At larger deformation levels, the local *J*-integral exhibits a more pronounced rise over the thickness range from 1 mm to 3 mm compared to other positions close to the free surfaces, but the overall distribution still remains relatively moderate. For the 30° tilted pre-crack configuration, the local *J*-integral increases from a minimum value on the side with deep pre-crack, to a maximum value close to the side with shallow pre-crack and then followed by a significant decrease. The distribution of the local *J*-integral is less uniform across the specimen thickness, leading to a much smaller minimum value and much larger maximum value. It is clear that the tilt angle of the pre-crack front mainly redistributes the local *J*-integral variation across the

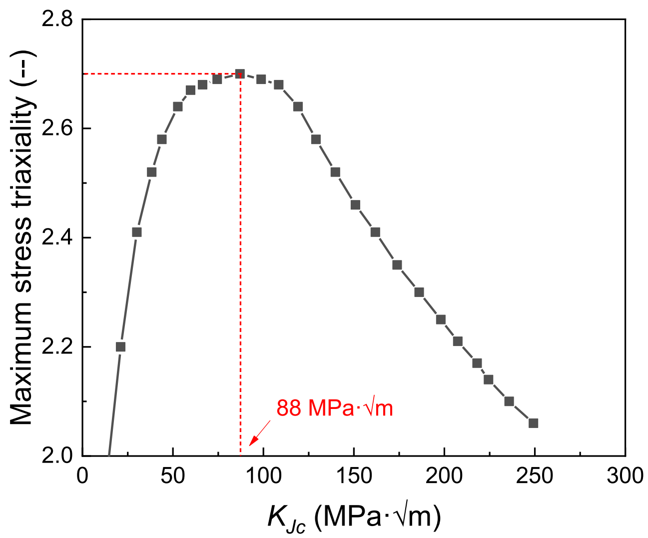

Fig. 6. Variation of maximum stress triaxiality ahead of pre-crack front with K_{Jc}.

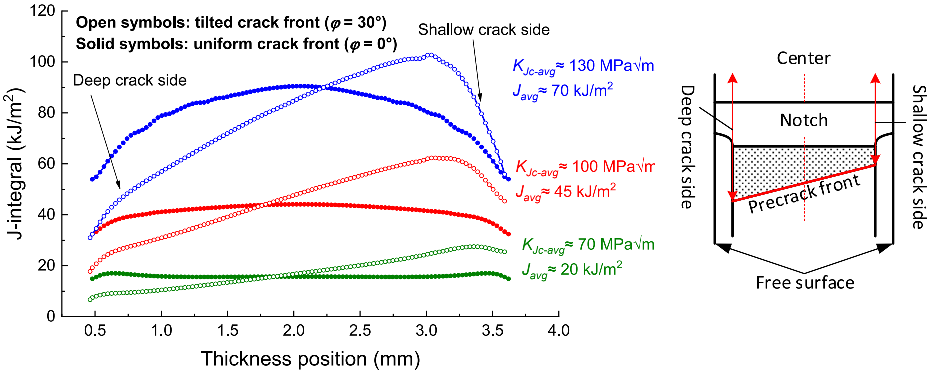

Fig. 7. Local J-integral distribution along uniform and tilted pre-crack front.

specimen thickness rather than modifying the global J-integral (see Fig. 5-b).

Additional understanding of the effect of pre-crack non-uniformity on brittle fracture can be gained by examining the distribution of the maximum principal stress along the specimen ligament. Fig. 8 shows that the variations of the maximum principal stress with the distance from the crack tip are generated at different thickness positions along the pre-crack front for the mini-CT specimen. As shown in Fig. 8(a), the thickness position $x/B_N = 1/64$ indicates the position closest to the free surface of the specimen, the thickness position $x/B_N = 1/2$ indicates the mid-thickness position, the other thickness positions are uniformly distributed between them. In these plots, the maximum principal stress is normalized by the material yield strength, σ_0, the distance from the crack tip is normalized by (J/σ_0) with J expressing the current J-integral. Two load levels $J = 20$ kJ/m^2 ($K = 70$ MPa$\sqrt{m}$) and $J = 70$ kJ/m^2 ($K = 120$ MPa$\sqrt{m}$) are considered, the first load level corresponds to the small scale yielding condition, whereas the latter load level corresponds to a well-contained yielding which is close to the fracture initiation in the experiments. Note that the J-integral in the following analysis are all computed using the analytical method in the ASTM E1820 based on the load-CMOD data.

The results displayed in Fig. 8(b-e) reveal that the distribution of the maximum principal stress has a strong dependence on the crack front position. At $J = 20$ kJ/m^2, for both pre-crack configurations, the maximum principal stress is maintained at the mid-thickness position over the distance range $1 \le r\sigma_0/J \le 3$, which is significantly larger than that close to the free boundaries ($x/B_N = 1/64$ & $63/64$). The normalized maximum principal stress at the mid-thickness position ($x/B_N = 1/2$) at $r\sigma_0/J = 2$ for the uniform pre-crack configuration is slightly larger than that for the tilted pre-crack configuration. It is worth noting that, due to the non-uniform local loading condition that is caused by the tilted pre-crack configuration, the distribution of maximum principal stress is not symmetrical about the mid-thickness plane, this feature becomes more obvious at higher load level.

At $J = 70$ kJ/m^2, the peak values of the maximum principal stress for both pre-crack configurations increase, whereas the value at $r\sigma_0/J = 2$ decreases due to an early loss of constraint in the mini-CT geometry at this level of loading. For the uniform pre-crack configuration, the maximum principal stress increases when it is closer to the mid plane of the specimen, with the maximum value observed at the mid-thickness position ($x/B_N = 1/2$). By contrast, for the tilted pre-crack configuration, the peak value of the normalized maximum principal stress spans over the thickness position range $x/B_N = 1/8$–$1/2$. While for the thickness positions on the other half of the crack front, the peak value is decreasing significantly as it is closer to the free surface. At the distance $r\sigma_0/J = 2$, which is generally considered to be the characteristic distance that indicates the crack tip constraint, the maximum value is observed to be located between the thickness positions $x/B_N = 3/8$ and mid-thickness position ($x/B_N = 1/2$). For the two thickness positions which are symmetrical about the mid plane, the maximum principal stress on the deep pre-crack side ($x/B_N = 1/64$, $1/8$, $1/4$) is larger than that on the shallow initial crack side ($x/B_N = 63/64$, $7/8$, $3/4$).

Apparently, the variation exhibited by the maximum principal stress indicates a clear effect of pre-crack non-uniformity. While the maximum principal stress level for both pre-crack configurations is comparable (with only a slightly lower value for the tilted pre-crack configuration), the distributions differ. For the uniform pre-crack configuration, the maximum principal stress is maintained at a higher level mainly at the mid-thickness position, for the tilted pre-crack configuration, the higher level of the maximum principal stress slightly shifts towards the deep crack side.

Similarly, another factor that has a direct impact on the initiation of brittle fracture is the development of the fracture process zone, which is also affected by the pre-crack inclination. Fig. 9 displays the contour maps of the maximum principal stress on the specimen remaining ligament, the white area and the grey area show the fracture process zone ($\sigma_{yy} \ge 2\sigma_0$ as defined in the local approach) at two K levels, $K = 70$ MPa$\sqrt{m}$ and $K = 120$ MPa$\sqrt{m}$, respectively. For the uniform pre-crack configuration, under small scale yielding condition, the fracture process zone is already well developed to a large proportion of the remaining ligament plane. With the increase of the load level, the extent of the process zone occurs more in the region close to the mid-thickness position. For the tilted pre-crack configuration, the process zone is also well developed under small scale yielding condition and is broadly uniformly distributed along the crack front. However, the spread of the process zone contrasts markedly with that for the uniform pre-crack configuration, the process zone grows more obviously in the area from the mid-thickness position to the deep pre-crack side. The observations on the extension of the fracture process zone might result in a deviation in the initiation position of the brittle fracture. The large maximum principal stress and the rapidly expanding fracture process zone between the mid-thickness and the deep pre-crack side indicates that

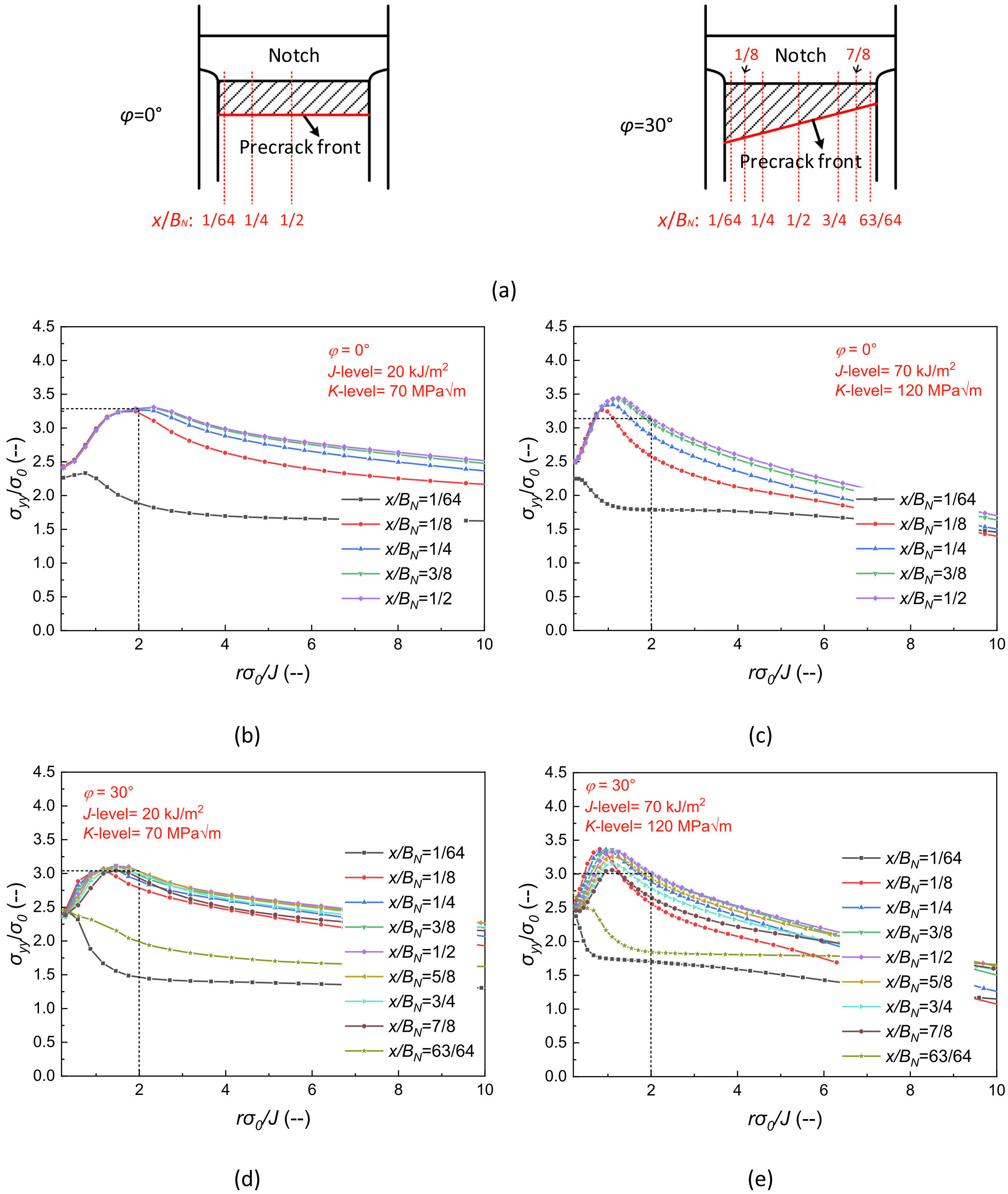

Fig. 8. (a) Schematic drawing of the normalized thickness positions for the uniform and tilted crack front. Distribution of maximum principal stress at $J = 20$ kJ/m^2 as a function of the normalized distance from a (b) uniform and (c) tilted pre-crack front. The distribution of maximum principal stress at $J = 70$ kJ/m^2 as a function of the normalized distance from a (d) uniform and (e) tilted pre-crack front.

the fracture initiation position for the tilted pre-crack configuration is located in this region. Hence closer to the deep crack side rather than at the mid-thickness position.

Instead of investigating the local stress distribution and the high stressed zone distribution, Fig. 10 displays the evolution of the fracture process zone size of the whole specimen, Ω, with the increase of the fracture toughness, K_J. It provides a quantitative description of the potential for both pre-crack configurations to trigger brittle fracture. The fracture process zone size of the uniform pre-crack configuration is larger than that for the tilted pre-crack configuration from the small scale yielding condition to the large scale yielding condition. The initiation of brittle fracture requires the attainment of a critical value which is controlled by the crack

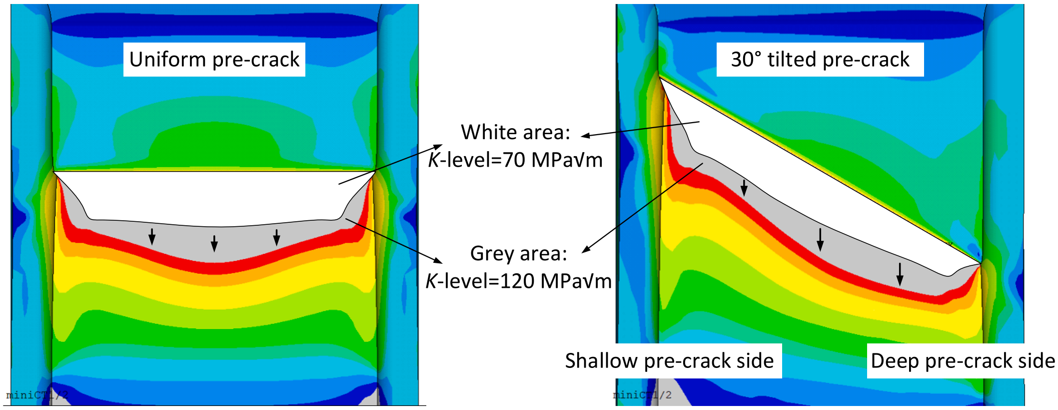

Fig. 9. The extension of the fracture process zone on the remaining ligament in front of uniform and tilted pre-crack front.

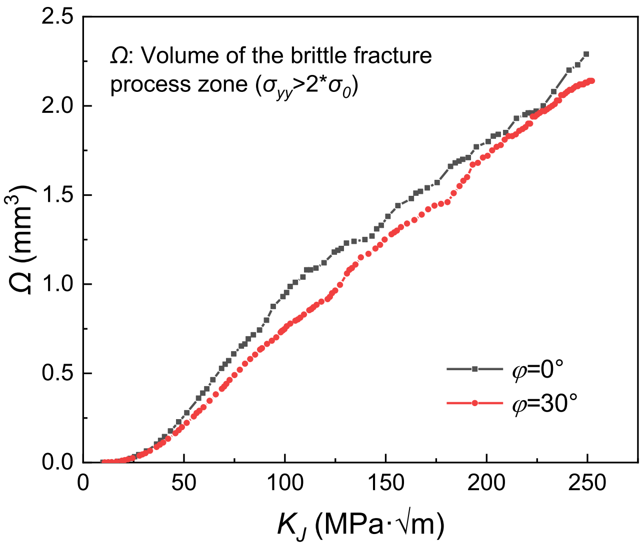

Fig. 10. Variation of the fracture process zone volume with increased loading ahead of uniform and tilted pre-crack.

front maximum principal stress and the fracture process zone size. A larger fracture process zone size in front of the uniform pre-crack configuration provides more favorable conditions to trigger brittle fracture. Moreover, as illustrated above, the peak value of the maximum principal stress for both pre-crack configurations are comparable (see Fig. 8). Similar maximum principal stress level occurs at smaller volume of the fracture process zone might result in not enough micro-cracks being sampled. Thus, this suggests that the fracture toughness for the uniform pre-crack configuration could potentially be lower than in non-uniform crack configuration. The question now comes to the quantitative impact of the pre-crack non-uniformity on the fracture toughness of mini-CT geometry, and whether it is still within engineering tolerance. In the next section, a local approach will be adopted to quantify the influence and further answer the questions.

5. Effect of pre-crack non-uniformity on the initiation of brittle fracture

5.1. Local approach to brittle fracture

The investigations of the macroscopic parameters reveal a potentially higher fracture toughness in a non-uniform pre-crack configuration. In order to go deeper and generalize quantitative understanding of the effect of pre-crack non-uniformity, a local approach to brittle fracture incorporating the effect of plastic strain is adopted for the estimation of the fracture toughness to be expected from non-uniform pre-crack configurations. That is, the particle distribution model, which is well used for analyzing the size effect of test specimens, was developed from the standard Beremin model [15]. Unlike the standard Beremin model, this model assumes that only a portion of all fractured particles eventually contribute to the brittle fracture process. A particle fracture stress was proposed to describe the effect of plastic strain on the failure probability. The particle distribution model is expressed as:

$$\sigma_w = \left[\frac{1}{V_0}\int_{\Omega}\left\{1-\exp\left[-\left(\frac{\sigma_{pf}}{\sigma_{prs}}\right)^{\alpha_p}\right]\right\}\sigma_1^m d\Omega\right]^{\frac{1}{m}}, \tag{2}$$

where σ_w is the Weibull stress, σ_{prs} is the particle reference stress, which represents an approximate average of the distribution of particle fracture stress in the given material, α_p is the Weibull modulus, which generally takes the value of 4 for ferritic structural steels [15], σ_{pf} is the particle fracture stress, $\sigma_{pf} = \sqrt{1.3\sigma_1 \epsilon_p E_d}$, in which ϵ_p is the effective matrix plastic strain and E_d represents the particle's elastic modulus, $E_d = 400$ GPa for the particles found in ferritic steels.

As already addressed in the relevant study of the new size correction scheme to determine fracture toughness [21], two parameters i.e., the Weilbull shape parameter, m, and the particle reference stress, σ_{prs}, need to be identified for the later calculation of σ_w. The Weibull parameter, m, is firstly determined to be equal to 21, which closely matches the values reported in previous studies [14,22,23]. This value is adopted as a fixed value in the subsequent investigations. Note that another value of the m factor within the acceptable range for this class of materials would lead to equally acceptable results because of the second parameter to which it is related. The second parameter, the particle reference stress, σ_{prs}, is identified at $-110\,^{\circ}$C based on the toughness scaling model (TSM). The model is based on the σ_w - K_{Jc} trajectories that are computed from the FEM analysis on the geometries with different constraint level. It is

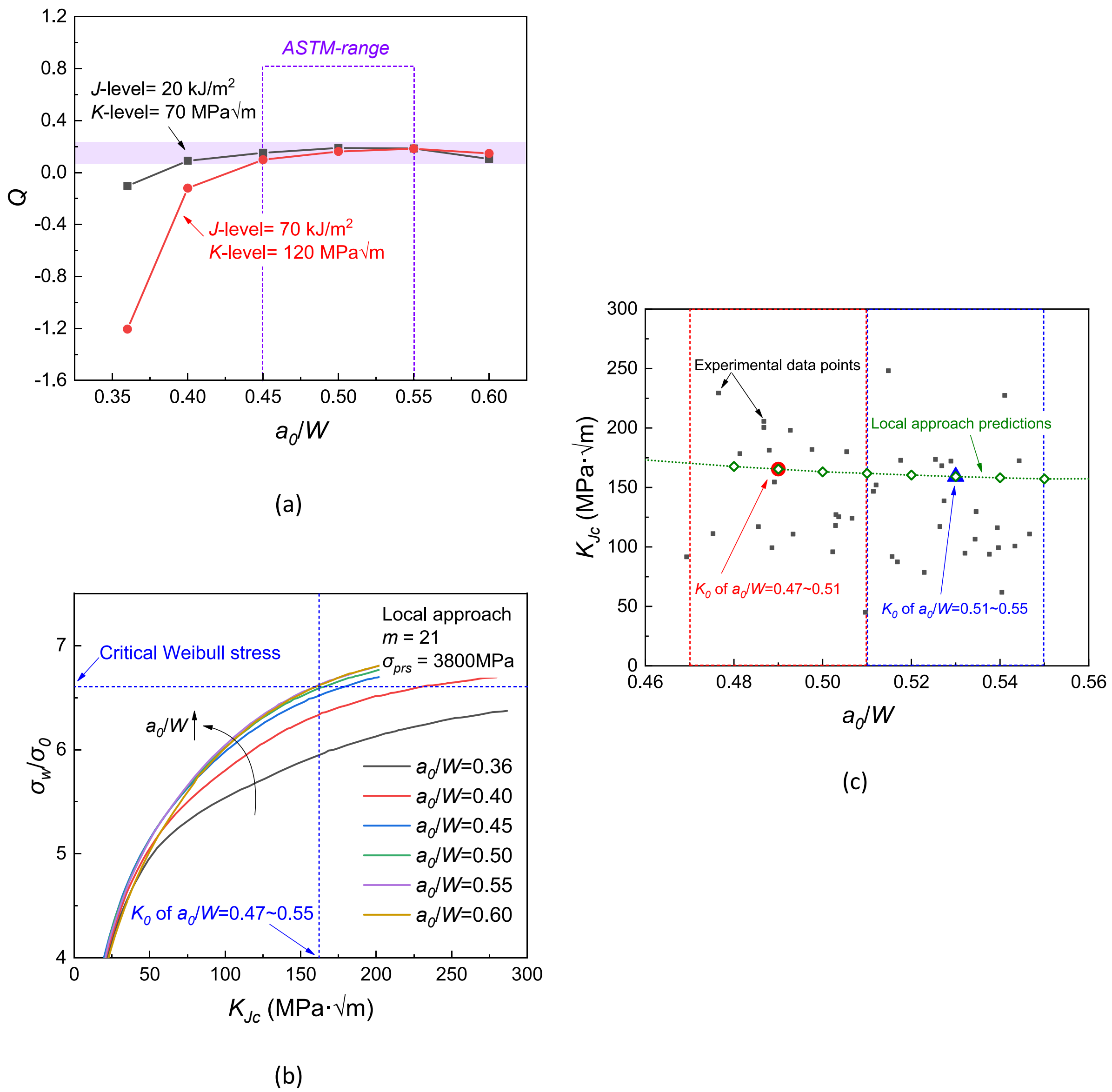

Fig. 11. (a) Variation of the Q parameter with initial crack size. (b) Variation of σ_w/σ_0 as a function of loading for the mini-CT specimens with various pre-crack size. (c) Experimental data and prediction results of the mini-CT specimens with various pre-crack size.

assumed that the brittle fracture is triggered when a certain critical Weibull stress is reached, even though different geometries have different fracture toughness values due to differences in constraints. By converting the $K_{Jc,0.5T\text{-}CT}$ and $K_{Jc,4T\text{-}CT}$ to their 1T size equivalence based on the size correction formulae given in the ASTM standard, a σ_{prs} value is obtained to give the best agreements of the σ_w-1T normalized K_{Jc} trajectories at −110 °C for the 4T-CT, 2T-CT, 1T-CT and 0.5T-CT geometries with the fixed m factor and σ_{prs}. That is, each σ_w-1T normalized K_{Jc} curve provides the same K_{Jc} value in the large CT geometries which produce the same Weibull stress, thus equal failure probability. The σ_{prs} then yields the value $\sigma_{prs} = 3800$ MPa. Subsequent studies demonstrated that the local approach, calibrated based on this method, can provide good constraint correlations between $K_{0,mini\text{-}CT}$ and $K_{0,1T\text{-}CT}$ [21]. These evidences thus support the adoption of the calibrated local approach on the mini-CT geometry which experiences significant loss of constraint and large effect of plastic strain.

The measured fracture toughness value is directly affected by the crack tip constraint, which varies with the initial crack length. The a_0/W ratio varies from 0.386 to 0.614 at different thickness positions in front of a 30° tilted pre-crack configuration, thus incorporating the effect of the initial crack length. To verify the capability of the calibrated local approach to analyze the tilted pre-crack configuration, this part describes the application of the local approach to predict the effect of the initial crack length on fracture toughness of the mini-CT geometry. First, as shown in Fig. 11(a), quantitative understanding of the effect of initial crack length can be obtained by examining the crack tip constraint using the J-Q methodology [24,25]. The Q parameters generated at the normalized distance $r\sigma_0/J = 2$ in front of the pre-cracks with different a_0/W vary from 0.35 to 0.6. Under small scale yielding condition (K-level = 70 MPa$\sqrt{\text{m}}$), almost all the initial pre-crack configurations have relatively high crack tip constraint levels, with the Q parameter between −0.1 and 0.2. In particular, the effect of a_0/W can be considered limited in the a_0/W range from 0.4 to 0.6. As the deformation level increases, under the large-scale yielding condition, the mini-CT geometries with initial crack size $a_0/W \leq 0.4$ show remarkably smaller crack tip constraint, with the Q parameter below 0. The constraint in front of deep pre-crack configurations ($a_0/W \geq 0.45$) is maintained at a relatively higher level of around 0.15. Meaningful fracture toughness value relies on higher crack tip constraint, the negligible change in the Q parameter when $a_0/W \geq 0.45$ meets the requirements in the ASTM standard regarding the initial crack size. For the 30° tilted pre-crack configuration, around 25% of the thickness of the specimen has an a_0/W ratio lower than 0.45, the fracture toughness value provided by this portion of pre-crack can thus be larger.

Fig. 11(b) provides the σ_w - K_{Jc} trajectories generated from the FEM models of deeply pre-cracked mini-CT specimens with a_0/W from 0.45 to 0.55. In this Figure, σ_w is normalized by the material yield strength, σ_0, at −110 °C, and local approach parameters with m = 21 and $\sigma_{prs} = 3800$ MPa are adopted. The plot clearly shows that the variation in the curves due to the constraint difference can be described by the calibrated local approach, even for the highly constrained pre-crack configurations with $a_0/W = 0.45 \sim 0.60$. For a certain critical Weibull stress, shallower pre-crack configurations correspond to larger predicted fracture toughness values due to lower crack tip constraint as expected from the J-Q theory. This feature becomes more significant when a_0/W is less than 0.45, and becomes negligible when a_0/W is larger than 0.45. The negligible deviation of the σ_w - K_{Jc} trajectories when $a_0/W \geq 0.45$ suggests that the crack tip is sufficiently constrained to provide stable fracture toughness value, which is consistent with the requirements in ASTM E1921 regarding the initial fatigue pre-crack size. This further demonstrates that the constraint difference due to initial crack size can be well described by the calibrated local approach.

The comparison between the prediction results based on the local approach and the experimental data are shown in Fig. 11(c). However, the mini-CT specimens were not tested at the same temperature. In order to provide sufficient data points to reveal the effect of pre-crack size, a simple procedure which assumes that each specimen follows its own master curve is applied to correct the measured fracture toughness at different temperatures to their equivalence at −110 °C. Since the K_{Jc} limit is beyond the scope of this paper, all data points are used in this part without any size correction and data censoring. Most of the a_0/W ratio of the tested mini-CT specimens are well within the required range from 0.45 to 0.55, as shown in the figure, these data points are then treated separately into two groups: $a_0/W = 0.47 \sim 0.51$ and $a_0/W = 0.51 \sim 0.55$. The scale fracture toughness, K_0, of these two groups of data points are 165.4 kJ/m^{2}and 159.2 kJ/m^2, respectively. It is observed that the K_0 of deeper pre-crack configurations is about 6 kJ/m^2 lower, showing a slight

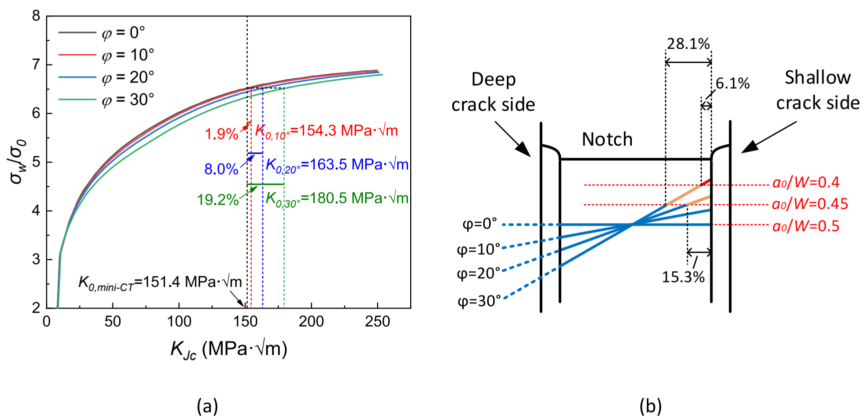

Fig. 12. (a) Evolution of σ_w/σ_0 with increased loading for the mini-CT specimens with uniform pre-crack and various tilted pre-cracks. (b) Proportion of different a_0/W involved in the tilted pre-crack configuration.

constraint dependence. The toughness scaling procedure between the mini-CT specimens with different pre-crack size is performed based on the K_0 value of $a_0/W = 0.47 \sim 0.51$, and this K_0 value is assumed as the fracture toughness of the pre-crack with an average $a_0/W = 0.49$. Prediction results (green curve) showing that the fracture toughness value decreases slightly with the increase of pre-crack length. The predicted fracture toughness value at $a_0/W = 0.53$ yields the value of 159.1 kJ/m^2, which is remarkably close to the K_0 value corresponding to $a_0/W = 0.51 \sim 0.55$. Therefore, the local approach with the parameters $m = 21$ and $\sigma_{prs} = 3800$ MPa can describe the effect of the constraint difference that is caused by the variation of pre-crack length. Thus, it is applicable for the simulation of the tilted pre-crack configurations which includes different pre-crack length conditions.

5.2. Fracture toughness predicted from different crack front configurations

In this section, the local approach model is applied to study the effect of pre-crack non-uniformity on the fracture toughness of the mini-CT geometry. Fig. 12 shows the evolution of σ_w / σ_0 under increasing values of K_{Jc} for the mini-CT geometries with uniform pre-crack and tilted pre-cracks with tilt angle of $\varphi = 10^\circ$, 20° and 30°. In the plot, the Weibull stress, σ_w, is computed based on the finite element simulations coupled with the local approach for brittle fracture. The fracture toughness, K_{Jc}, is computed using the procedure given in ASTM E1820 which is based on the load-CMOD curves generated from tests. It is clear that, for a given load level as characterized by the K_{Jc}, σ_w decreases with increasing tilt angle. The decrease of the Weibull stress becomes more obvious at a large tilt angle. To go further, a quantitative measure of the effect of tilt angle is proposed. The Weibull fitting parameter, K_0, as a parameter that plays a role in the distribution of measured fracture toughness data, is considered to be a characteristic value of different geometries in the toughness scaling model. Previously, a Master Curve of mini-CT geometry was established based on a large number of fracture test data, the transition temperature, T_0, was determined to be -107 °C, which is considered to be reasonable compared to that determined from large standard CT geometries. The K_0 value generated from the Master Curve yields the value of 151.4 MPa/m at -110 °C. As a scale parameter that sufficiently characterizes the K_{Jc} value of mini-CT at corresponding temperature, this value is identified as the fracture toughness of the mini-CT with reference pre-crack configuration, that is, the mini-CT with uniform pre-crack configuration.

Based on the toughness scaling methodology, the K_0 value determined from the Master Curve is corrected to its equivalent characteristic toughness for the mini-CT geometry with 10°, 20° and 30° tilted pre-crack front. The K_0 for these three tilted pre-crack configurations at -110 °C then yield the values of 154.3 kJ/m^2, 163.5 kJ/m^2 and 180.5 kJ/m^2, respectively. The difference between the predicted K_0 values and the reference value ($K_0 = 151.4$ MPa$\sqrt{\text{m}}$) are 1.9%, 8.0% and 19.2% respectively. The discussion about the tilted pre-crack configuration indicated that the near-tip highly stressed zone close to the shallow pre-crack side tends to be not fully developed, thus leading to higher fracture toughness. Therefore, the difference in the fracture toughness value can be explained by the proportion of shallow cracks contained in the pre-crack front. As illustrated above, the crack tip constraint in front of a shallow pre-crack tends to be lower and the fracture toughness is therefore overestimated, the overestimation of the toughness value is enhanced when a_0/W is lower than 0.45. As shown in Fig. 12(b), for the 10° titled pre-crack, the a_0/W of the pre-crack ranges from 0.465 to 0.535, the a_0/W of the entire pre-crack is larger than the ratio of 0.45. For the 20° titled pre-crack, the a_0/W of the pre-crack ranges from 0.428 to 0.572, 15.3% of the pre-crack has the a_0/W lower than 0.45; for the 30° titled pre-crack, the a_0/W of the pre-crack range from 0.386 to 0.614, 28.1% of the pre-crack has a a_0/W lower than 0.45, 6.1% of the pre-crack has a a_0/W lower than 0.4. Clearly, the 30° tilted pre-crack configuration has the largest proportion of the pre-crack with a_0/W below 0.45, which is around two times more than that for the 20° tilted pre-crack configuration. Moreover, for the 30° tilted pre-crack configuration, 6.1% of the pre-crack with a_0/W lower than 0.4 further increases the deviation of the fracture toughness. Thus, the K_0 difference of 19.2% for the 30° tilted pre-crack configuration has a significant increase compared to the 8.0% difference caused by the 20° tilted pre-crack configuration.

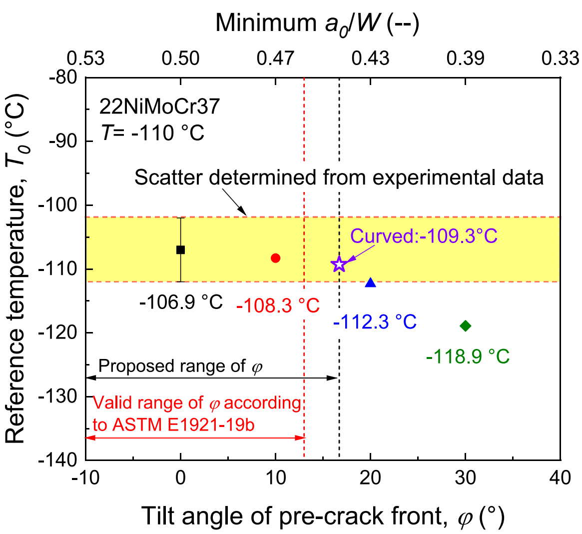

Fig. 13. Reference temperature (T_0) evaluated from the uniform pre-crack configuration and various tilted pre-crack configuration.

Further understanding of the effect of pre-crack non-uniformity on the fracture toughness of mini-CT geometry can be gained by examining the computed transition temperature, T_0. For the reference group, $T_0 = -106.9$ °C was determined previously according to the calculation formulae given in section 10 in the ASTM E1921-19b, which is based on a large number of test data of mini-CT specimens at different temperatures. The uncertainty band of ± 5 °C was determined based on the margin adjustment approach given in section 10 in the ASTM E1921-19b, which considers the uncertainty in T_0 that is associated with the sample size and experimental uncertainties, etc. [8]. As for other pre-crack configurations, T_0 is computed based on the determined K_0 using Eq.(3) and Eq. (4).

$$K_{Jc(med)} = 20 + 0.91(K_0 - 20), \tag{3}$$

$$T_0 = T - \left(\frac{1}{0.019}\right) ln\left(\frac{\left(K_{Jc(med)} - 30\right)}{70}\right). \tag{4}$$

As shown in Fig. 13, T_0 is equal to −108.3 °C, −112.3 °C and −118.9 °C, respectively, for 10°, 20° and 30° tilted pre-crack configurations. According to the requirements in ASTM E1921-19b, the acceptable tilt angle for the valid pre-crack front should not exceed 13°. The T_0 generated from the 20° tilted pre-crack configuration, which should have been considered invalid, falls right on the lower limit of the uncertainty band defined by the experimental data. The T_0 generated from the 30° tilted pre-crack configuration falls outside of the uncertainty band, indicating an unacceptable value.

Therefore, the validity limit of the tilt angle for this kind of voluntarily exaggerated, academic-research-use pre-crack front is around 20° (with $a_0/W = 0.428 \sim 0.572$). The maximum deviation of the local pre-crack length from the average pre-crack length is 0.6 mm, exceeding the validity limit of $\pm 0.1(b_0B_N)^{1/2}$ given in the ASTM standard by 63%. Moreover, in previous discussions [11], the pre-crack front curvature can be described by the C factor:

$$C = \frac{\max|a_0 - a_i|}{(b_0B_N)^{0.5}}, \tag{5}$$

where a_0 is the average fatigue pre-crack length, a_i is the pre-crack length measurement at any of the nine physical measurement points as indicated in ASTM E1921 ($i = 1 \sim 9$). According to ASTM E1921-19b [8], the C factor of a valid pre-crack front should not be larger than 0.1. However, the above discussions indicate that T_0 is not significantly affected when C is smaller than 0.16. Therefore, the existing restrictions on the mini-CT geometry regarding the pre-crack front curvature are not necessary and can be relaxed without significant effects on the fracture toughness results. Lambrecht et al. [6] proposed that the two outer points in the nine point measurement can be discarded in the examination of pre-crack front curvature, that is, only apply the $\pm 0.1(b_0B_N)^{1/2}$ validity criteria on the seven inner points. This criterion reduces the invalid percentage from 8% to 6% without affecting the final results. The application of the $\pm 0.1(b_0B_N)^{1/2}$ validity criteria on the 7 inner points (with $a_0/W = 0.44 \sim 0.56$) yields the tilt angle of 16.7° (see Fig. 13), which is a little conservative compared to the limit tilt angle of 20° in this study. But the investigations conducted in this paper demonstrating that the criteria proposed by Lambrecht et al. [6] is reliable and feasible. Based on the newly proposed criteria, after excluding the two external measurement points, the recommended validity limit of the C factor for the seven inner points can be recalculated as 0.1 ($i = 2 \sim 8$ in Eq.5). The maximum allowable value is 0.12, which corresponds to a tilt angle of 20°.

It should be noted however that only the portion of pre-crack with a_0/W lower than 0.45 has a significant effect on setting the magnitude of the fracture toughness. As illustrated above, 15.3% of the 20° tilted pre-crack configuration has the a_0/W lower than 0.45. It is reasonable to demonstrate that this portion can be considered as another factor to determine the validity of the pre-crack front. In other words, the percentage of the pre-crack front with a_0/W lower than 0.45 plays a stronger role on the qualification of the pre-crack front. In particular, the real non-uniform pre-crack fronts on the mini-CT specimens are generally smooth, only with one

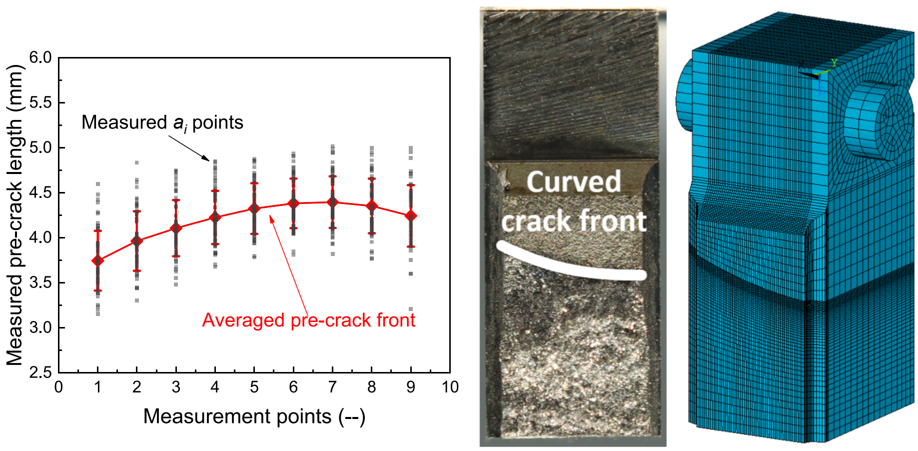

Fig. 14. The shape of a typical invalid pre-crack front and its corresponding finite element model.

or two points close to the specimen surfaces below the lower validity limit. Examining the pre-crack front in terms of the "valid crack percentage" rather than applying validity limit on the physical measurement points allows more efficient use of the mini-CT K_{Jc} data that would otherwise be considered invalid.

In order to verify the efficiency of the proposed crack front relaxation of the pre-described requirements, finite element analysis was conducted on a mini-CT with a more realistic curved pre-crack front. The shape of the analyzed pre-crack front was obtained from the average trend of the measurements of 60 invalid pre-crack fronts determined according to the requirements in ASTM E1921-19b. The resulting shape of a typical invalid pre-crack front, along with a finite element model featuring a similar pre-crack shape, is shown in Fig. 14. The selected crack front shape is curved and different from the tilted crack front analyzed in this paper. However, unlike the usually observed valid quasi-straight pre-crack front, it has a maximum and a minimum crack length close to the two ends of the crack front. Finally, the curved pre-crack front in the finite element model was selected to precisely comply with the proposed requirements of pre-crack front curvature, which was $\pm 0.1(b_0B_N)^{1/2}$ at the 7 inner measurement points. The results show that the K_0 for the curved pre-crack configuration at −110 °C is equal to 156.5 kJ/m^2, and the calculated T_0 is equal to −109.3 °C (see Fig. 13), which is remarkably close to the results obtained from the 10° tilted pre-crack configuration. For a more realistic curved pre-crack with only the measured crack length at one point exceeding the validity limit, the generated T_0 still remains within the uncertainty band. Compared to the tilted pre-cracks, the curved pre-crack does not exhibit a significant effect on T_0. It is important to note that our investigation of the curved pre-crack configuration is limited to the most commonly observed invalid pre-crack shape, but experimental evidence based on real cracks with much more tortuous fronts support those conclusions [1]. Our findings clearly demonstrate that the proposed relaxation of the standard requirements with respect to crack non-uniformity presented in this paper can ensure the generation of stable fracture toughness values, even in the presence of curved pre-cracks.

6. Summary and conclusions

Given the limited thickness of the mini-CT geometry, non-uniform pre-crack often tends to develop during fatigue pre-cracking. As a result, a large number of mini-CT specimens can result in invalid data due to the existing strict requirements regarding pre-crack size, thus leading to a waste of test resources. Previous experimental investigations on the pre-crack non-uniformity have demonstrated a weak effect of non-uniform crack front on fracture toughness. This paper describes numerical investigations about the effect of pre-crack non-uniformity on the stress fields and fracture toughness of mini-CT geometry in the ductile-to-brittle transition (DBT) region. For this purpose, a local approach to brittle fracture which was demonstrated to provide reliable predictions of fracture behavior in the test specimens with a diverse range of crack tip constraint was applied. Finite element simulation results on the uniform pre-crack configuration and the tilted straight pre-crack configuration suggest that:

- Pre-crack non-uniformity has a negligible effect (less than 3%) on the maximum load and *J*-integral. Instead, the effect mainly lies in the local *J*-integral, the maximum principal stress and the fracture process zone:
  - For the tilted pre-crack configuration, the local *J*-integral shows larger value near the side with the shallow pre-crack.
  - The half specimen near the deep crack shows larger maximum principal stress than that of the other half, the fracture process zone on this half is also more extended.
  - The fracture process zone volume in front of the uniform pre-crack configuration is larger than that for the tilted pre-crack configuration.
- A local approach model to brittle fracture is used to study the effect of pre-crack non-uniformity on the initiation of the brittle fracture. The results show that the tilt angle of 10°, 20° and 30° increase the predicted fracture toughness, K_{Jc}, by 1.9%, 8.0% and 19.2%, respectively. The reference temperature, T_0, is reduced by 1.3 °C, 5.3 °C and 12.0 °C, respectively.
- Larger apparent fracture toughness is expected from the pre-crack with $0.35 \leq a_0/W < 0.45$, smaller and invariant fracture toughness is expected from the pre-crack with $0.45 \leq a_0/W \leq 0.6$. The increase of the K_{Jc} value of the tilted pre-crack configurations is mainly dependent on the relative proportion of shallow pre-crack with respect to the whole crack front.

Overall, the research conducted in the present study shows that the effect of pre-crack non-uniformity on the fracture toughness of mini-CT geometry becomes significant when the tilt angle exceeds 20°, although beyond the existing validity limit of pre-crack front curvature given in ASTM E1921-19b. The present study suggests that the restrictions on the pre-crack front curvature can be relaxed. The analysis on the realistic curved pre-crack configuration suggests that the methodology of applying the validity limit of $\pm 0.1 (b_0B_N)^{1/2}$ on the seven inner points [6] (with minimum $a_0/W = 0.44$ and $C = 0.1$) is an effective option in this context.

CRediT authorship contribution statement

Meng Li: Conceptualization, Data curation, Formal analysis, Investigation, Methodology, Validation, Visualization, Writing – original draft, Writing – review & editing. **Inge Uytdenhouwen:** Writing – review & editing, Supervision, Software, Data curation, Project administration, Resources. **Thomas Pardoen:** Writing – review & editing, Supervision. **Rachid Chaouadi:** Writing – review & editing, Supervision, Software, Resources, Project administration, Data curation. **Marlies Lambrecht:** Writing – review & editing, Data curation.

Declaration of Competing Interest

The authors declare that they have no known competing financial interests or personal relationships that could have appeared to influence the work reported in this paper.

Data availability

Data will be made available on request.

Acknowledgements

The present work was performed within the SUSTAIN project at SCK CEN supported by the NMS management. In addition, part of the work was done under the FRACTESUS project that has received funding from the Euratom research and training program 2020-2024 under grant agreement No. 900014. The authors gratefully acknowledge the support of the technical staff of LHMA at SCK CEN. The authors also acknowledge SCK CEN Academy for PhD funding. Additionally, the authors would like to acknowledge the late Dr. Tomasz Brynk for his extensive contributions to this work.

References

[1] Chaouadi, R., R. Gérard, and E. van Walle. *Fracture toughness characterization of vessel forging with hydrogen flaked specimens*. in *ASME 2016 Pressure Vessels and Piping Conference*. 2016. American Society of Mechanical Engineers, PVP2016-63632.
[2] Chaouadi, R., M. Lambrecht, and R. Gérard. *Crack Resistance Curve Measurement With Miniaturized CT Specimen*. in *ASME 2018 Pressure Vessels and Piping Conference*. 2018. American Society of Mechanical Engineers, PVP2018-84690.
[3] Chaouadi, R., et al. *On the use of miniaturized CT specimens for fracture toughness characterization of RPV materials*. in *ASME 2016 Pressure Vessels and Piping Conference*. 2016. American Society of Mechanical Engineers, PVP2016-63607.
[4] Scibetta, M., *Constraint assessment in miniature C (T) specimens using 3D finite element simulations*, in *SCK CEN Report BLG-923*. 2002.
[5] Lucon E, Scibetta M, Chaouadi R, van Walle E, Dean SW. Use of miniaturized compact tension specimens for fracture toughness measurements in the upper shelf regime. J ASTM Int 2006;3(1):13235.
[6] Lambrecht M, Chaouadi R, Li M, Uytdenhouwen I, Scibetta M. On the Possible Relaxation of the ASTM E1921 and ASTM E1820 Standard Specifications with Respect to the Use of the Mini-CT Specimen. Mater Perform Charact 2020;9(5):20190217.
[7] Li, M., et al., *Investigations on the effect of pre-crack non-uniformity for the mini-CT geometry during ductile fracture.* Submitted, 2023.
[8] ASTM, *ASTM E1921-19b*, in *Standard Test Method for Determination of Reference Temperature, T_0, for Ferritic Steels in the Transition Range*. 2020, ASTM International: West Conshohocken, PA.
[9] ASTM, *ASTM E1921-18a*, in *Standard Test Method for Determination of Reference Temperature, T_0, for Ferritic Steels in the Transition Range*. 2019, ASTM International: West Conshohocken, PA.
[10] Li, M., et al., *Effect of the pre-crack non-uniformity on the initiation of brittle fracture in a mini-CT*, in *IGRDM-Update*. October, 2021, SCK CEN: Online.
[11] Lindqvist S, Kuutti J. Sensitivity of the Master Curve reference temperature T0 to the crack front curvature. Theor Appl Fract Mech 2022;122:103558.
[12] Bridgman P. The stress distribution at the neck of a tension specimen. Trans. Am. Soc. 1944.
[13] Anderson, T.L., *Fracture mechanics: fundamentals and applications*. 2017: CRC press.
[14] Gao X, Ruggieri C, Dodds R. Calibration of Weibull stress parameters using fracture toughness data. Int J Fract 1998;92(2):175–200.
[15] Ruggieri C, Dodds Jr RH. An engineering methodology for constraint corrections of elastic–plastic fracture toughness–Part I: A review on probabilistic models and exploration of plastic strain effects. Engng Fract Mech 2015;134:368–90.
[16] Ruggieri C, Savioli RG, Dodds Jr RH. An engineering methodology for constraint corrections of elastic–plastic fracture toughness–Part II: Effects of specimen geometry and plastic strain on cleavage fracture predictions. Engng Fract Mech 2015;146:185–209.
[17] Pardoen T, Hutchinson J. An extended model for void growth and coalescence. J Mech Phys Solids 2000;48(12):2467–512.
[18] Petti JP, Dodds Jr RH. Calibration of the Weibull stress scale parameter, σu, using the Master Curve. Engng Fract Mech 2005;72(1):91–120.
[19] Enterprise, A.M., *Understanding Fracture Mechanics*. Help System. Release 2023 R1: ANSYS, Inc.
[20] Shih CF, Moran B, Nakamura T. Energy release rate along a three-dimensional crack front in a thermally stressed body. Int J Fract 1986;30(2):79–102.
[21] Li, M., et al., *Size correction scheme to determine fracture toughness with mini-CT geometry in the transition regime.* Submitted, 2023.
[22] Andrieu A, Pineau A, Besson J, Ryckelynck D, Bouaziz O. Beremin model: Methodology and application to the prediction of the Euro toughness data set. Engng Fract Mech 2012;95:102–17.
[23] Wasiluk B, Petti JP, Dodds Jr RH. Temperature dependence of Weibull stress parameters: Studies using the Euro-material. Engng Fract Mech 2006;73(8): 1046–69.
[24] O'Dowd N, Shih CF. Family of crack-tip fields characterized by a triaxiality parameter—I. Structure of fields. J Mech Phys Solids 1991;39(8):989–1015.
[25] O'Dowd NP, Shih CF. Family of crack-tip fields characterized by a triaxiality parameter—II. Fracture applications. J Mech Phys Solids 1992;40(5):939–63.